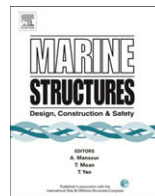




Contents lists available at ScienceDirect

Marine Structures

journal homepage: www.elsevier.com/locate/marstruc



Structural stability of polymer matrix composite panels in fire

Pei Gu^{a,*}, Ming Dao^b, R.J. Asaro^c

^aMSC Software Corporation, 6050 Scripps Street, San Diego, CA 92122, United States

^bDepartment of Materials Science and Engineering, Massachusetts Institute of Technology, Cambridge, MA 02139, United States

^cDepartment of Structure Engineering, University of California at San Diego, CA 92093-0085, United States

ARTICLE INFO

Article history:

Received 12 October 2008

Received in revised form 20 April 2009

Accepted 21 April 2009

Keywords:

Polymer matrix composite

Single skin panel

Sandwich panel

Structural integrity in fire

ABSTRACT

Development in advanced composite fabrication technology offers the clear prospect of cost effective application of polymer matrix composites for large load-bearing structures. However, polymer matrix composites can be severely degraded under the thermal condition caused by fire. This paper addresses the compressive load-bearing capacity for polymer matrix composite panels in naval structures and civil infrastructures under the combined thermal–mechanical condition. The failure modes arising from structural instability for single skin and sandwich panels in such combined thermal–mechanical condition are the focus in this study. The thermal field under fire heating and the degradation of mechanical properties with elevated temperature are discussed. Analytical solutions for these mechanical failure modes are presented for design considerations. The approach to the development of a quantitative methodology for fire protection design is discussed in the context of the analyses and the experiments. Design diagrams are constructed to design mechanical loads for given fire protection time, and on the opposite, to design fire protection time for given mechanical loads.

© 2009 Elsevier Ltd. All rights reserved.

1. Introduction

Advanced manufacturing technology offers clear prospects for polymer matrix composites to be used as large load carrying structures. The advantage is that such composites are *designer materials*

* Corresponding author.

E-mail addresses: pei.gu@mscsoftware.com (P. Gu), mingdao@mit.edu (M. Dao), rasaro@san.rr.com (R.J. Asaro).

wherein their properties and performance can be optimized. Compared with conventional construction materials, such as steel and aluminum, advanced composites offer high specific strength and stiffness, high fatigue and corrosion resistance, as well as significant reduction in weight. The concern associated with the use of polymer matrix composites as construction materials for naval structures is their fire performance [1]. The composites can be severely degraded under thermal loading caused by fire. This temperature-dependent behavior reduces mechanical load carrying capacity and thus can lead to structural failure under operational loads designed without the consideration of fire damage. On the other hand, due to low thermal conductivity, thermal gradient exists for a long period of heating time such that material gradient, e.g. the variation of Young's modulus with position, exists in the temperature-dependent materials. This makes the mechanical behavior of the non-homogeneous materials to be different from that of homogeneous materials. To discuss the failure mechanism and the design of the composite, the mechanical fields, stresses and deformation, need to be evaluated considering the effect of the material gradient induced by the thermal gradient.

Due to the above, the understanding of the composites' mechanical performance in the combined thermal-mechanical loading environment is an ongoing interest. A physical model that is originated from naval applications is a panel made of such composites subjected to in-plane compressive mechanical load and transverse thermal gradient caused by fire. A research program carried out in various institutes, including the structural engineering department at the University of California at San Diego, intends to evaluate the polymer matrix composite panels (FRP panels) for fire protection, see Reference [1]. The investigation includes following aspects: (1) characterization of temperature profiles under typical thermal boundary conditions; (2) characterization of material degradation that describes material behavior in the elevated temperature; (3) modeling the structural collapse to determine the critical status for the components and systems; (4) establishment of sound design criteria for structural integrity in fire.

In the early works of fire damage to the polymer matrix composites, the chemical decomposition at sufficiently high temperature, which results in the loss of mass and charring, was considered in the thermal model to explore failure mechanisms [2,3]. In addition to heat conduction, the thermal model accounts for the generated or absorbed heat as well as the generated volatile gases in the decomposition of the polymer matrix. This thermal model was used in the combined thermal-mechanical analyses to explore the mechanical failure mechanisms. In References [4,5], a two-layer model, which divided the thickness into a thermally affected portion with reduced mechanical properties and an unaffected portion with the virgin-state mechanical properties in room temperature, was used to model the mechanical failure of the composites. In References [6,7], a refined layer model, which has a number of layers for evaluating the temperature-dependent mechanical properties, was used to study the tensile strength and compressive strength.

Over the past years, our work has been focused on the fire damage to the structural's mechanical performance so that the appropriate measure can be taken for fire protection in the design stage. Our early portion of the study was on the thermal-mechanical testing and the comparison of the testing with the finite element modeling [8–10]. Later, rigorous approaches, closed-form solutions and detailed modeling, have been sought to capture the combined thermal-mechanical process accurately [11–16]. Design methodology for the composite panels was discussed in References [9,10,17,18]. The purpose of this paper is to further discuss the stability issues for the polymer matrix composite panels in the combined fire and mechanical load condition, from the design considerations. From this point of view, it is an overview of our previous work in this area. We analyze the developed technique for evaluating the stability of polymer matrix composite panels in the combined one-sided heat and compressive mechanical load. In the examples, by constructing the design diagrams we illustrate such technique may be used for designing the composite panels in naval structures. The design procedure utilizes the analytical solutions for the panels with material properties' gradients induced by the temperature gradient and temperature-dependent material behavior [11,13], obtained from the theory of non-homogeneous materials or functionally graded materials. The failure modes to be discussed are buckling for the single skin panel and the sandwich panel; skin wrinkling for the sandwich panel. We will not address micromechanical failure mechanisms such as micro-cracking, delamination and micro-buckling, which were observed and discussed in References [6,19]. To design reusable panels, the composite materials are assumed to be in the virgin state in the combined thermal-mechanical

loads, say, the temperature is below 300 °C. The chemical decomposition at higher temperature and associated permanent damages, i.e. charring and the loss of mass, are not considered here for this design purpose. However, the discussed methodology is extendible to include the chemical decomposition by employing the thermal model investigated in References [2,3,16].

The plan of this paper is as follows. In Section 2, the transverse temperature field caused by fire heating and the material degradation at elevated temperature are discussed. A simple mathematical expression in power form is employed to capture the material degradation with an experimentally determined parameter. In Section 3, the analytical solution of buckling load that considers the material gradient is discussed in detail for single skin panels. In Section 4, the analytical solution of buckling load that considers the material gradients in both the skins and the core is discussed in detail for sandwich panels. It includes the additional effect induced by the shear of the core due to its finite shear stiffness [20]. In Section 5, the analytical solution of skin-wrinkling load is presented for sandwich panels. There are two cases discussed for the wrinkling solution. The first case considers the material gradients in both the skin and the core, assuming that the material gradient in the core follows an exponential form and the thickness of the core is much larger than that of the skin. The second case considers the finite thickness of the core and the material gradient in the skin, whereas the material gradient in the core is neglected. Each of the above solutions is presented in a separated section so that it can be read independently.

In Section 6 of the paper, we briefly discuss the thermal–mechanical testing of the composite panels and compare the testing result with the analytical solution for the failure mode of buckling. In Section 7, the combined thermal–mechanical process is simulated by the chained thermal–mechanical process: the temperature field is first obtained from the heat transfer analysis using the finite difference method; then, is substituted into the above analytical solutions to determine the critical loads. The scheme of the computer program developed for the simulation is discussed. Examples are given to construct design diagrams to locate allowable mechanical load-bearing capacity, allowable temperature and fire protection time for given thermal and mechanical requirements. In the last section, Section 8, we summarize the approach to assess the failure modes of buckling and skin wrinkling. Other failure modes, those caused by non-uniform thermal expansion and external forces, are briefly discussed.

2. Material degradation and temperature distribution

Assuming the composites are in the virgin state, the variation of Young's modulus with temperature is given by a phenomenological form,

$$E(T) = \begin{cases} E_0 \left(1 - \frac{T - T_r}{T_{ref} - T_r} \right)^m & \text{for } T_r \leq T \leq T_{ref}; \\ 0 & \text{for } T \geq T_{ref}. \end{cases} \quad (1)$$

Here, E_0 is Young's modulus at the ambient temperature T_r ; T_{ref} is the reference temperature at which Young's modulus vanishes. The power index m can be taken between 0 and 1, with $m = 0$ being no degradation below the reference temperature T_{ref} . The temperature dependent form Equation (1) is empirical and obtained by fitting thermal–mechanical test data. The power form expression is plotted into curves in Fig. 1 along with the test data for E-glass fiber/vinylester matrix composites given in References [9,10]. It is evident that among the three curves in the figure the test data close to that for $m = 0.2$. The power form for temperature-dependent material behavior was also suggested in Reference [21] (page 97). Similar decreasing behavior for Young's modulus with temperature was used in Reference [19]. The degradation of the material's mechanical properties Equation (1) is referred as material degradation law. Since the material is in the virgin state, Equation (1) implies that the degradation in material properties, or thermal softening, is reversible. The degradation law overlooks the stiffness when the temperature is above the reference temperature, by treating it as zero. Test data given in References [9,10] suggest that $T_{ref} = 120$ °C and the stiffness is sufficiently small to be neglected above the reference temperature. The material is said to be completely degraded when the temperature is above the reference temperature.

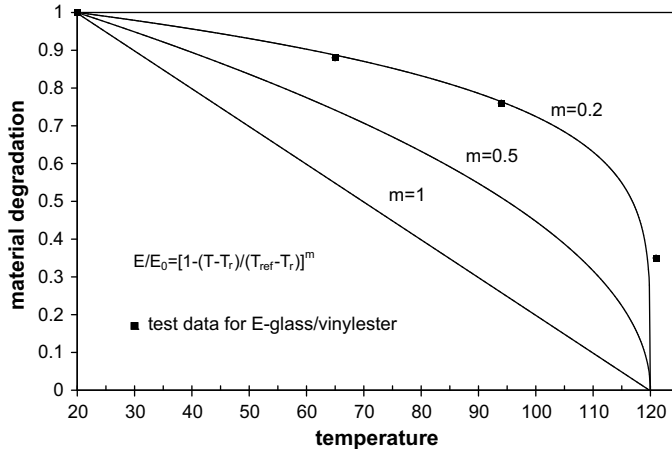


Fig. 1. Material degradation law in power form. The figure shows the degradation as a function of elevated temperature for different power indices and the comparison with experimental data for E-glass/vinylester composites.

Material variation with position y along the thickness of the panel can be obtained by substituting the temperature field $T(y,t)$ into Equation (1) assuming that the temperature field is independent of the x , where t is the heating time and x and y are coordinates. The x axis is along a in-plane direction and the y axis is along the thickness direction, with the y coordinate being zero at the exposed face. One can expand the material variation into the polynomial of y by omitting the higher order terms,

$$E(y) = Ay^2 + By + C. \tag{2}$$

Consider the single skin panel and denote the moduli at the exposed face, the center, and the unexposed face as E_f , E_c and E_b , respectively. The coefficients in Equation (2) are given by interpolation as

$$A = \frac{2(E_b - E_f) - 4(E_c - E_f)}{h^2},$$

$$B = \frac{4(E_c - E_f) - (E_b - E_f)}{h},$$

$$C = E_f. \tag{3}$$

Note that the three moduli in Equation (3) are temperature dependent according to Equation (1). Other forms for the material variation with position may also be introduced, e.g. the exponential form discussed in Reference [13]. These simplified forms allow analytical solutions to be presented in compact forms [11–13].

Due to the temperature-dependent material behavior, one needs to know the temperature distribution in order to determine the material properties for structural analysis. The thermal gradient is presented for a long period of heating time due to the low thermal conductivities for materials such as E-glass fiber/vinylester matrix composites. Knowing the thermal properties, i.e. conductivity and specific heat, one can obtain temperature field by solving the heat conduction equation with prescribed boundary conditions and initial conditions. The temperature field may also be obtained from thermal tests. The temperature field across the thickness of the single skin panel is smooth; the temperature field across the thickness of the sandwich panel is piecewise smooth, smooth in each of the skin and the core. The temperature field for both types of panels decreases from the fire exposed face to the unexposed face. The initial condition is the ambient temperature, or room temperature. Uniform

heating at the exposed face, which represents the case in thermal tests, is considered such that the heat transfer problem becomes one-dimensional. In the thermal tests [9,10], mineral wood was used as insulation at the exposed face and uniform heat flux into the panel was achieved. Thermocouples were placed at the exposed face, the center and the unexposed face to measure the temperature histories.

Let the thermal conductivity be $K(T)$; the specific heat C_p ; the mass density ρ . The one-dimensional heat conduction equation is

$$\frac{\partial}{\partial y} \left[K(T) \frac{\partial T(y, t)}{\partial y} \right] = \rho C_p \frac{\partial T(y, t)}{\partial t}. \quad (4)$$

The thermal boundary condition at the exposed face is the measured or specified temperature versus time curve $T(0, t) = T_f(t)$. At the unexposed face, the thermal boundary condition is either the measured temperature versus time curve $T(h, t) = T_b(t)$ or the insulation type $\partial T(h, t) / \partial y = 0$. When the temperature field is known, the material properties are determined through the material degradation law Equation (1), or Equations (2) and (3). As mentioned in Introduction section, the heat transfer analysis does not consider the chemical decomposition at high temperature since we focus on the virgin state of the polymer matrix. For considering the charred state at high temperature, the thermal model studied in References [2,3,16] needs to be employed.

In Reference [10], we obtained numerical solutions of the temperature field for representative panels made of E-glass/vinylester composites by solving the heat conduction Equation (4) using the measured temperatures at the exposed face and unexposed face in thermal tests. Based on these solutions, simplified temperature distributions were discussed. The simplified temperature distributions allow us capture the major features of the actual temperature fields and the temperature variations using the temperature values measured at the key locations in thermal tests. For single skin panels, a two-parameter model was proposed, which used two of the following temperature values to construct the linear temperature profile: temperatures at the exposed face, the center and the unexposed face. Fig. 2 shows the comparison of the temperature field obtained by solving the heat conduction equation with that of the two-parameter model for a single skin panel.

For the simplified temperature distribution of sandwich panels, the temperature at the unexposed skin can be taken as ambient temperature because the low conductivities keep the unexposed skin with small amount of temperature elevation for a considerable period of heating time. Fig. 3 systematically shows a piecewise step distribution of the temperature field derived from the actual temperature field. The step distribution results in piecewise step variation of material properties according to the material degradation law Equation (1). The three temperature values that characterize the simplified distribution are the temperature at the exposed face, the temperature at the interface between the exposed skin and the core, and ambient temperature at the unexposed skin. It can be called upper bound temperature field because the above temperature values are the maximum temperatures in the skins and the core, respectively.

3. Buckling of single skin panel

The structural panel is shown in Fig. 4(a) where the mechanical load is for the panel to subject the in-plane compression. The thermal gradient caused by fire presents along the thickness due to low thermal conductivity of polymer matrix composites. Buckling load derived in Reference [11] is discussed in this section for the single skin panel.

A one-dimensional beam model is considered such that the width of panel is taken to be a unit value, i.e. $b = 1$. Because of the material gradient induced by thermal gradient, the neutral axis is not located at the center of the cross-section, as shown in Fig. 4(b). We apply the Bernoulli–Euler assumption such that the cross-section remains plane and rotates about the neutral axis during the bending deformation. The position of the neutral axis is obtained from equilibrium as

$$y_0 = \frac{\int_0^h F[T(y), m] y dy}{\int_0^h F[T(y), m] dy}, \quad (5)$$

for the general material variation form, Equation (1). In Equation (5),

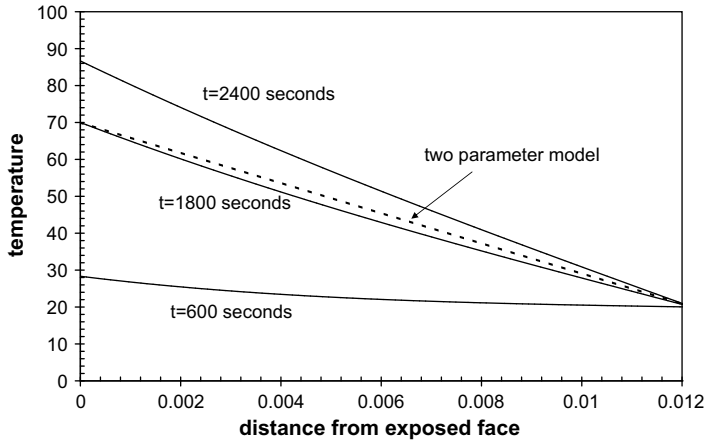


Fig. 2. Temperature field for the single skin panel. The temperature field of the two-parameter model is plotted to compare with the actual temperature field. The two-parameter model is an approximation to the actual temperature field.

$$F[T(y), m] = \left(1 - \frac{T(y) - T_r}{T_{ref} - T_r} \right)^m \tag{6}$$

Using Equation (2), the position of the neutral axis is

$$y_0 = \frac{3Ah^3 + 4Bh^2 + 6Ch}{4Ah^2 + 6Bh + 12C} \tag{7}$$

The resultant moment M of the cross-section, defined positive as shown in Fig. 4(b), is

$$M = \int_0^h \sigma_{xx}(y - y_0) dy = \kappa \int_0^h E(y)(y - y_0)^2 dy = \kappa D(T) \tag{8}$$

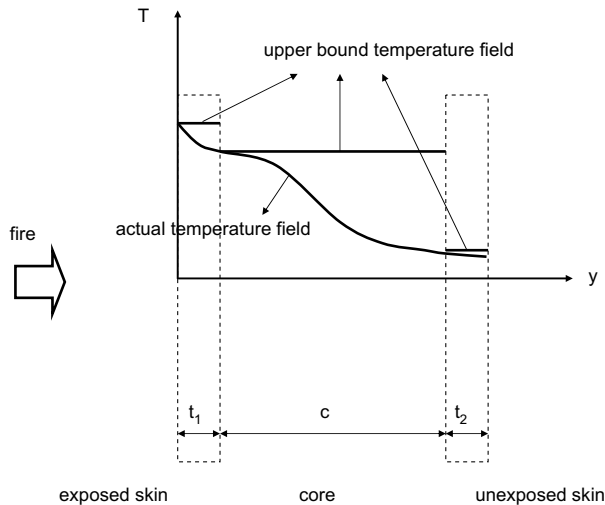


Fig. 3. Temperature field and thermal gradient for the sandwich panel. The actual temperature field is piecewise smooth across the entire thickness of the sandwich panel. The upper bound temperature field is a step function obtained by taking the maximum temperature values in the skins and the core, respectively.

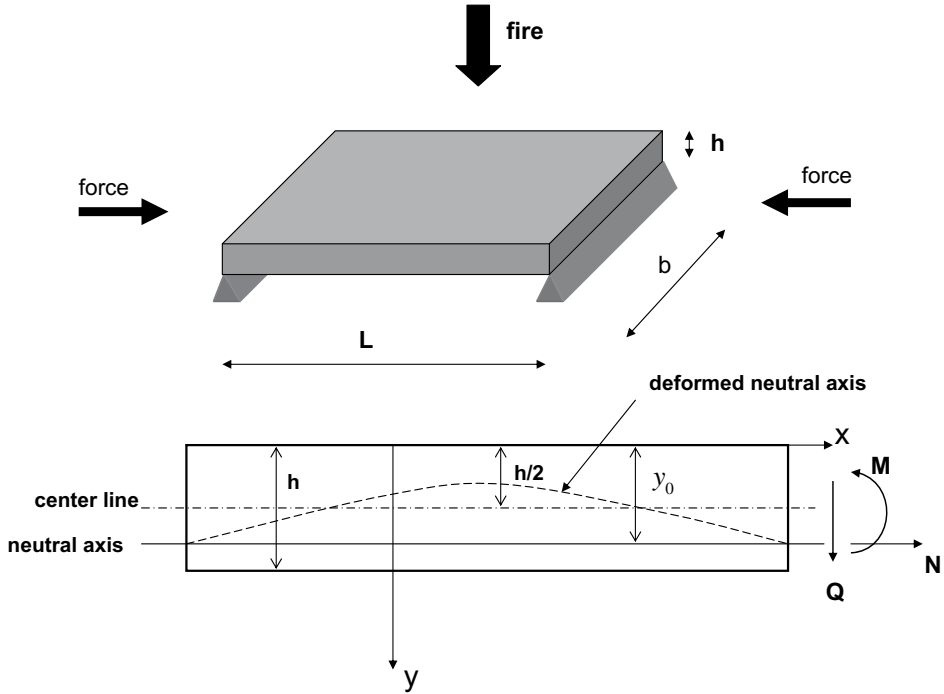


Fig. 4. (a) Thermal–mechanical model for the panel. (b) The bending moment and shear force on the cross-section; the location of the neutral axis for bending deformation.

Here $\kappa = -\partial^2 u_y(x)/\partial x^2$ is the curvature of the deformed neutral axis. In Equation (8), D is the bending stiffness for the graded material,

$$D(T) = \int_0^h E(y)(y - y_0)^2 dy. \tag{9}$$

For temperature independent material, $D = E_0 I$, where $I = h^3/12$ is the bending moment of inertia for the panel. If Equation (1) is employed, we have

$$D(T) = E_0 \int_0^h F[T(y), m](y - y_0)^2 dy. \tag{10}$$

The bending stiffness is denoted by $D(T)$ since it relates to the temperature field.

From the formulation, the equilibrium equation for the bending deformation is of the same form as that for homogeneous materials except the expression of the bending stiffness. This leads to the buckling load for the non-homogeneous materials to be is of the same form as that for homogeneous materials. For roller supports (pin supports which allow rotation) at both ends, the buckling load is give by

$$P_{cr} = \pi^2 \frac{D(T)}{l^2}. \tag{11}$$

Here, l is the length of the panel. This shows that the temperature gradient, *via* material gradient, reduces the critical load through the reduction of the bending stiffness $D(T)$. For clamping supports at both ends (do not allow rotation), the coefficient π^2 in Equation (11) is replaced by $4\pi^2$. For one end with roller support and the other end with clamping support, the coefficient π^2 in Equation (11) is replaced by 4.49^2 .

The above expression may be scaled by the buckling load of temperature independent materials, or homogeneous materials, to write as

$$P_{cr} = \frac{\pi^2 E_0 h^3}{12I^2} D^*(T). \tag{12}$$

Here, $D^*(T)$ is non-dimensional bending stiffness. In general, the full temperature field is needed to obtain P_{cr} where the evaluations of the associated integrals in Equations (5) and (10) may need to be done numerically. Note that Equations (11) and (12) are applied to the case that no portion is completely degraded, Fig. 5(a). If a portion is completely degraded, Fig. 5(b), the effective thickness h^* needs to be used to replace h .

Several observations can be made from the above solution. First, the buckling load is explicitly expressed by the temperature field and is not explicitly related to the thermal properties, e.g. thermal conductivity and specific heat. This tells us that if the two composite panels have the same geometrical dimensions and the same material degradation law, the buckling load is the same for both panels as far as the thermal boundary conditions give rise to the same temperature field. Second, the reduction factor from initial buckling load $D^*(T)$ is only dependent on temperature field, not geometrical dimensions. In other words, if two panels made from the same composite have different lengths, widths and thicknesses but have the same temperature distribution, the percentage of reduction from initial buckling load is the same for both panels. The third observation is that $D^*(T)$ decreases as temperature increases. The following two special values are known: $D^*(T) = 1$ when the heating time $t = 0$; $D^*(T) = 0$ when the entire thickness reaches the reference temperature. The fourth observation is that the buckling load can be tailored through the changing of the geometrical dimensions. Same as homogeneous materials or temperature independent materials, the buckling load is proportional to the thickness of the panel and inversely proportional to the length of the panel.

4. Buckling of sandwich panel

For sandwich panels with material gradients along the thickness, the location of the neutral axis is obtained from Equation (5) as

$$y_0 = \frac{\int_0^{t_1} E_{of} F[T(y), m_f] y dy + \int_{t_1+c}^{t_1+t_2+c} E_{of} F[T(y), m_f] y dy + \int_{t_1+c}^{t_1+c} E_{oc} F[T(y), m_c] y dy}{\int_0^{t_1} E_{of} F[T(y), m_f] dy + \int_{t_1+c}^{t_1+t_2+c} E_{of} F[T(y), m_f] dy + \int_{t_1+c}^{t_1+c} E_{oc} F[T(y), m_c] dy}, \tag{13}$$

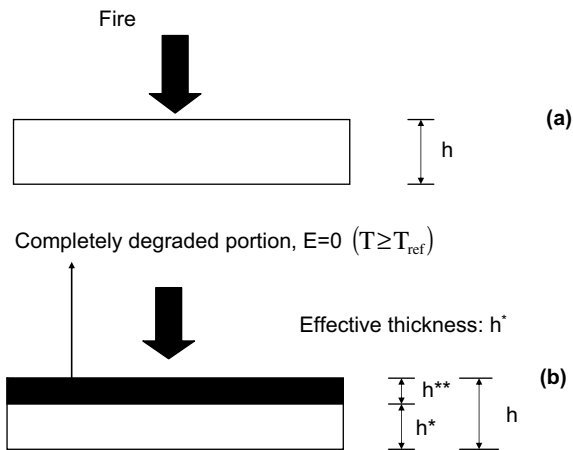


Fig. 5. The effective thickness h^* should be used in evaluating load-bearing capacity when a portion at the exposed side h^{**} is completely degraded.

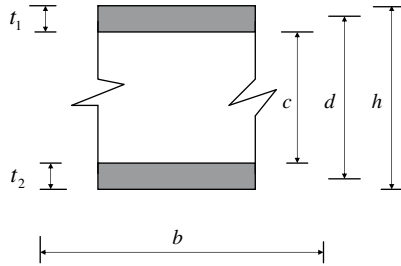


Fig. 6. The cross-section in a sandwich panel. When $t_1 = t_2$, it is symmetric panel; when $t_1 \neq t_2$, it is un-symmetric panel. The b is the width of the panel; the d is the distance between the centers of the two skins.

In Equation (13), c , t_1 and t_2 are the thicknesses of the core and the skins, as shown in Fig. 6. The E_{0f} and E_{0c} are Young’s moduli of the skin and the core at ambient temperature; the m_f and m_c are the power indices of the skin and the core in the material degradation law Equation (1).

For the sandwich panels, the finite shear stiffness of the core introduces additional shear deformation, as shown in Fig. 7. The additional shear deformation reduces the buckling load obtained from standard bending theory. We write the total deflection as

$$w(x) = w_1(x) + w_2(x), \tag{14}$$

where w_1 is the deflection obtained from standard beam theory; w_2 is the deflection induced by the shear of the core. The approach to include the shear of the core can be found in Reference [20]. Using the approach, for roller supports at both ends we derived the buckling load of sandwich panels with material variation due to the thermal gradient as [11]

$$P_{Cr} = P_E \frac{1 + P_{Ef}/P_c - (P_{Ef}/P_c)(P_{Ef}/P_E)}{1 + P_E/P_c - P_{Ef}/P_c}, \tag{15}$$

where

$$P_E = \frac{\pi^2 D}{l^2}; \quad P_{Ef} = \frac{\pi^2 D_f}{l^2}; \quad P_c = AG^*. \tag{16}$$

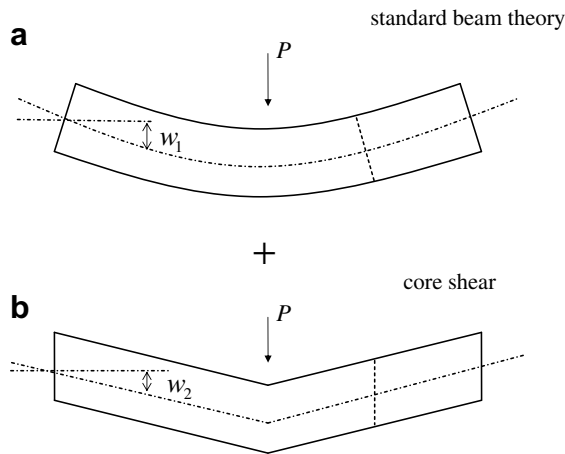


Fig. 7. Bending deformation in a sandwich panel is composed of two deformation modes: (a) the deflection by standard beam theory; (b) the deflection induced by the shear of the core. The actual deformation is the superposition of the two modes.

The buckling load of a sandwich panel with material gradient along the thickness is of the same form as that without gradient. The differences are the expressions for the bending stiffness of the panel D , the bending stiffness of the skins D_f , and shear stiffness of the core AG^* . For clamping supports at both ends, the π^2 in Equation (16) for P_E and P_{Ef} is replaced by $4\pi^2$. For one end with roller support and the other with clamping support, the π^2 in Equation (16) for P_E and P_{Ef} may be replaced by 4.49^2 .

In the above expressions, the bending stiffness of the panel is given by

$$D = \int_0^{t_1} E_{of} F [T(y), m_f] (y - y_0)^2 dy + \int_{t_1+c}^{t_1+t_2+c} E_{of} F [T(y), m_f] (y - y_0)^2 dy + \int_{t_1}^{t_1+c} E_{oc} F [T(y), m_c] (y - y_0)^2 dy. \tag{17}$$

The bending stiffness of the two skins about their own neutral axes is given by,

$$D_f = D_{f1} + D_{f2},$$

$$D_{f1} = \int_0^{t_1} E(y) (y - y_{01})^2 dy,$$

$$D_{f2} = \int_0^{t_2} E(y + t_1 + c) (y - y_{02})^2 dy, \tag{18}$$

where

$$y_{01} = \frac{\int_0^{t_1} F [T(y), m_f] y dy}{\int_0^{t_1} F [T(y), m_f] dy},$$

$$y_{02} = \frac{\int_0^{t_2} F [T(y + t_1 + c), m_f] y dy}{\int_0^{t_2} F [T(y + t_1 + c), m_f] dy} \tag{19}$$

The shear stiffness of the core is given by

$$AG^* = \frac{d}{c} \int_{t_1}^{t_1+c} G(y) dy. \tag{20}$$

Here, A is the cross-section area of the core and G^* is the averaged shear modulus of the core. The variation of $G(y)$ follows the same form as that for Young's modulus, Equation (1) or Equation (2).

For thin skins, we take $P_{Ef} = 0$ such that the expression (15) becomes

$$\frac{1}{P_{cr}} = \frac{1}{P_E} + \frac{1}{P_C}. \tag{21}$$

5. Skin wrinkling of sandwich panel

Skin wrinkling is the transverse deformation of the skin in the sandwich panel as shown in Fig. 8. Since the low stiffness of the core in the transverse direction, the panel may be in favor of such transverse deformation mode to lose stability. In Reference [13], the solutions for two cases were

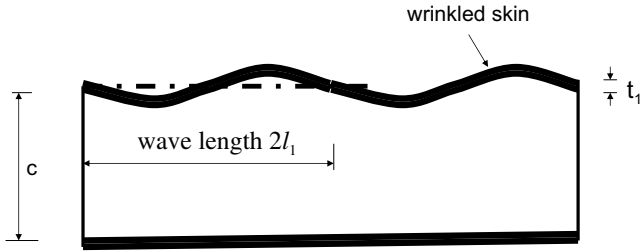


Fig. 8. Skin-wrinkling model of the sandwich panel. The deformation mode during wrinkling is in the form of sinusoidal waves.

obtained analytically by deriving the relationship between membrane stress in the skin that drives skin wrinkling and the wavelength of the wrinkled skin. The wrinkling load is the minimum of the membrane stress in terms of the wavelength.

The first case is that the thickness of the core is much larger than the thickness of the skin so that the core thickness is mathematically treated as infinity in solving the stress and deformation fields of the core. This allows only one skin to be considered in the mechanics model by neglecting the interaction between the two skins. This solution can be written as

$$\sigma_{cr} = B_1 E_{1c}^{\frac{2}{3}} E_{1s}^{\frac{1}{3}}, \tag{22}$$

where σ_{cr} is wrinkling stress. The wrinkling load is $2t_1 b \sigma_{cr}$, assuming each skin taking the same amount of load. The E_{1c} is Young's modulus of the core at the interface with the exposed skin; E_{1s} is Young's modulus of the exposed skin at the exposed face. The coefficient is

$$B_1 = 0.6751 D^{\frac{1}{3}} + 1.2599 D^{\frac{1}{3}} a^* (0.966\lambda) \frac{1}{\lambda}. \tag{23}$$

In Equation (23), $D^* = D_{f1} / (E_{1s} t_1^3)$ and

$$a^*(q) = \frac{2q \left(\frac{q}{2} - \sqrt{1 + \frac{q^2}{4}} \right)}{\nu_{1c}^2 - \left(\frac{q}{2} - \sqrt{1 + \frac{q^2}{4}} \right)^4 - 2(1 + \nu_{1c}) \left(\frac{q}{2} - \sqrt{1 + \frac{q^2}{4}} \right)^2}, \tag{24}$$

where ν_{1c} is Poisson's ratio of the core at the interface with the exposed skin. The critical wavelength defined as $q = \beta l_1 / \pi$ (l_1 is the half of the wavelength shown in Fig. 8) is

$$q = = 0.966\lambda = 0.966 \left(2D^* \frac{E_{1s}}{E_{1c}} \right)^{\frac{1}{3}} (\beta c) \frac{t_1}{c}. \tag{25}$$

As shown in Fig. 8, t_1 and c are the thickness of the skin and the core respectively. The material gradient of the core is

$$\beta c = \ln \frac{E_{2c}}{E_{1c}}. \tag{26}$$

The E_{2c} is Young's modulus of the core at the interface with the unexposed skin.

Using the above solution, we showed in Reference [13] that the material gradients in the core do not have strong effect on the wrinkling load by comparing wrinkling load obtained from the actual temperature field and that from the upper bound temperature field of the core. The upper bound temperature field of the core is a uniform temperature distribution that has the maximum temperature value of the actual temperature field in the core. The maximum temperature is achieved at the interface between the exposed skin and the core.

In the second case, the upper bound temperature field of the core is used. This allows us obtain the stress and deformation fields of the finite thickness core from a closed-form solution such that the interaction between the two skins can be considered. The critical stress is given in the same form as Equation (22) with the coefficient

$$B_1 = \left[2^{-\frac{2}{3}}\theta^2\lambda_1^2 + 2^{\frac{1}{3}}\frac{g(\theta)}{\lambda_1} \right] D^{*\frac{1}{3}} \tag{27}$$

In Equation (27),

$$\lambda_1 = \frac{t}{c} \left(2D^* \frac{E_{1s}}{E_{1c}} \right)^{\frac{1}{3}} \tag{28}$$

The normalized critical wavelength $\theta = \pi c/l_1$ is obtained from the nonlinear equation,

$$\lambda_1 = - \left[\frac{1}{\theta} \frac{dg(\theta)}{d\theta} \right]^{\frac{1}{3}} \tag{29}$$

In Equation (29),

$$g(\theta) = \frac{2}{\theta} \frac{(3 - \nu_{1c})\sinh \theta \cosh \theta + (1 + \nu_{1c})\theta}{(1 + \nu_{1c})(3 - \nu_{1c})^2 \sinh^2 \theta - (1 + \nu_{1c})^3 \theta^2} \tag{30}$$

Here, ν_{1c} is Poisson’s ratio of the core.

The solution for the first case considers the material gradients induced by thermal gradients in the skin and the core, but the thickness of the core is taken to be infinitely large in order to analytically obtain stress and deformation fields of the core. Note that the thickness of the core is in the solution, see Equations (25) and (26), since the thickness is necessary in defining the material gradient of the core β . In the solution for the second case, the upper bound temperature field of the core is used to obtain the wrinkling load that accounts for the finite thickness of the core. In the simulation in Section 7, both cases are evaluated and the smaller wrinkling load is chosen as the critical load in designing panels.

6. Experimental verification of buckling loads

In this section, we compare the analytical buckling load obtained in previous sections with available experimental results in the combined thermal–mechanical loading condition. We first briefly describe the experimental setting which can be found with more specific details in References [8,9]. The experiments were performed under ASTM E119 fire condition, i.e. following the E119 temperature–time history curve. The ends of the panel were with roller type condition to allow rotation. The test apparatus used hydraulic rams to apply both in-plane and out-of-plane loads. A small out-of-plane load, in the direction into the frame or away from the frame, was applied to simulate the initial imperfection of the panel. The fixture was bolted onto the rim of a furnace for fire exposure. The mineral wool was used at the exposed face as insulation to control the uniform heat flux into the panel. Thermocouples were placed at three locations along the thickness of the panel, the exposed face, the center and the unexposed face. The thermocouple at the center was co-molded in during the panel fabrication. This interior thermocouple, a mechanical defeat to the combined thermal–mechanical loading, was only used in the thermal tests to calibrate the temperature distribution.

For the single skin panels and the skins of the sandwich panels, the composites were composed of E-glass fabric, vacuum infused, in vinyl ester matrix; the cores of the sandwich panels were made of *airlite* foam. The dimensions of the single skin panel were the length $l = 0.9144$ m, the thickness $h = 0.012192$ m and the width $b = 0.7112$ m. For the sandwich panel, the skins were symmetric with the thickness $t_1 = 0.003556$ m; the thickness of the core was $c = 0.0127$ m. The mechanical property data were as follows. For the single skin panel and the skin of the sandwich panel, Young’s modulus at ambient temperature was $E_0 = 2.07 \times 10^{10}$ Pa. For the core, Young’s modulus at ambient temperature

was $E_{0c} = 6.624 \times 10^7$ Pa, whereas shear modulus at ambient temperature was $G_{0c} = 2.547 \times 10^7$ Pa. These mechanical properties may be found in Reference [10]. The power index for the material degradation law Equation (1) was $m = 0.2$ for both the E-glass/vinylester composite and the *airlite* foam. The reference temperature was taken as $T_{ref} = 120^\circ$ and ambient temperature $T_r = 20^\circ$ for both the single skin and the sandwich panels.

For single skin panels, we compare the buckling load discussed in Section 3 with test result given in Asaro et al. [10]. Fig. 7 of Reference [10] gave stiffness variation along the thickness for representative heating times, obtained by using the material degradation law and the temperature field. The temperature distribution was determined by solving the one-dimensional heat conduction equation with the prescribed E119 temperature versus time history. After 70 minutes of fire expose, the degradation in modulus in Fig. 7 of Reference [10] was: $E_f/E_0 = 0$, $E_c/E_0 = 0.65$ and $E_b/E_0 = 0.9$. With this, we determine the material variation from the expressions (2) and (3); then, evaluate the buckling load from Equations (9) and (11). The buckling load obtained this way is $P_{cr} = 9340$ N, which matches the finite element result given in Fig. 8 of Reference [10]. Following the same way, Fig. 9 (Fig. 9 of this paper) shows buckling loads at some heating times and the estimated buckling load curve obtained by connecting the discrete points with straight lines. The intersection of the buckling load curve and applied load curve is the failure point, which corresponds to the maximum fire protection time period. From the figure, the estimated failure time with applied in-plane compressive load at 6670 N is around 72 minutes, whereas the actual measured failure time from test is 65 minutes. Considering that the 1330 N out-of-plane load applied in the test to simulate initial imperfection of the panel, which would contribute to failure, and there may be difference between the end support condition in testing and end support condition for modeling, the match is fairly good. The measured deflection is also plotted in Fig. 9, which shows that near the failure time the deflection increases dramatically due to instability. The test data are in agreement with the analytical results for the failure time and buckling load.

For sandwich panels, the thermal distribution for representative heating times was known from Fig. 14(b) of Reference [10]. The buckling loads for the representative heating times are calculated from Equations (15)–(20), using the material degradation law Equation (1). The estimated buckling load curve is plotted in Fig. 10. The intersection of the buckling load curve and applied compressive load, 17,800 N, is the failure time, which corresponds to the maximum fire protection time period. Same as the single skin panel, there is an out-of-plane load applied for the sandwich panel, 890 N, to simulate the initial imperfection. Also plotted is the measured deflection for the same panel, which shows near the failure time, around 33 minutes, the deflection increases dramatically due to instability.

7. Design diagram

As described in Section 2, the temperature field is obtained from the solution of the heat conduction equation and the temperature-dependent material properties are determined from the material degradation law Equation (1). The buckling load and wrinkling load are then obtained from those solutions given in Sections 3–5. Design diagrams are constructed by plotting the failure loads versus heating time. The above procedure has been made into a computer program to automate the design process. The input data are the following for the panels: (1) thermal properties (thermal conductivity, specific heat, mass density); (2) mechanical properties (Young's modulus at ambient temperature, power index for material degradation law); (3) geometrical properties, the length, width and thickness. For the sandwich panels, the input includes the above mechanical properties for the core and the skins; the thicknesses of the core and the skins. In addition to these, the input is needed for locations of the grid points along the thickness of the panel where the temperature is calculated; the time step size to evaluate the critical load in the time domain. The thermal boundary conditions, the histories of temperature versus heating time at the exposed face and at the unexposed face, are inputted through either functional forms or discrete data. The reference temperature at which the material is completely degraded and ambient temperature needs to be inputted for both the skins and the core of the sandwich panels. The portion at the exposed side where temperature is above the reference temperature is removed from the calculation, or deactivated.

In the computer program, for each time step we first calculate the temperature field from the finite difference scheme for the heat conduction equation. When the temperature distribution is known at

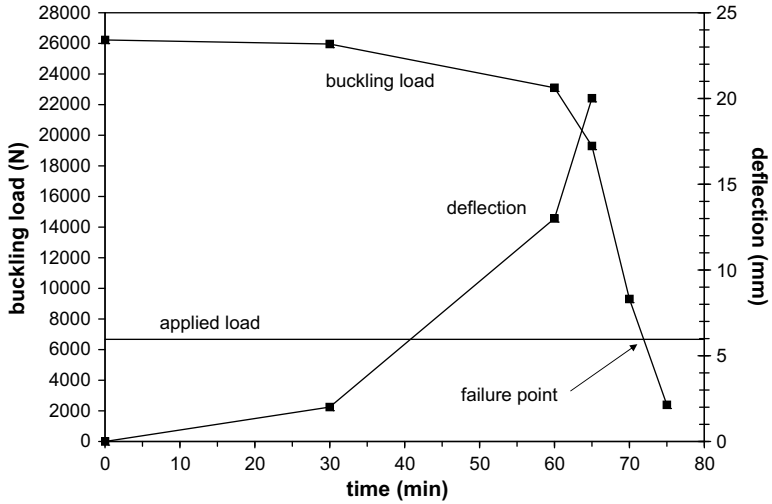


Fig. 9. The computed buckling load versus heating time for a single skin panel, where measured out-of-plane deflection and applied load are also plotted. The intersection of the buckling load curve with the applied load curve is the failure point, at which the deflection starts to increase dramatically in a short time period.

the time step, the material variation is known from the material degradation law. If this time step is that specified for evaluating critical loads, the buckling load and/or wrinkling load are calculated. The product of the program is a design diagram, a curve of critical load versus heating time. In the case of single skin panel, the critical load is the buckling load; in the case of sandwich panel, we choose the lowest of the buckling load and the wrinkling load. The design diagram can be outputted or kept in data storage for specific design search. If one gives the allowable mechanical load in a design requirement, the program locates the fire protection time from the design diagram and then the allowable temperature from the thermal boundary condition at the exposed face. On the other hand, if one gives the allowable temperature in a design requirement, the program locates the fire protection time from the thermal boundary condition and then the allowable mechanical load from the design diagram.

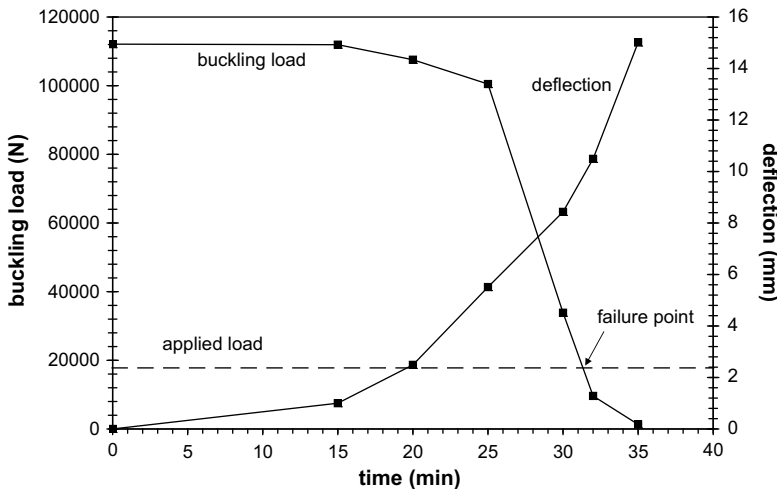


Fig. 10. The computed buckling load versus heating time for a sandwich panel, where measured out-of-plane deflection and applied load are also plotted. The intersection of the buckling load curve with the applied load curve is the failure point, at which the deflection starts to increase dramatically in a short time period.

To demonstrate the design procedure for structural fire protection, we consider the following thermal boundary conditions. The exposed face's temperature versus heating time curve is simplified as a linear relationship shown in Fig. 11 and the unexposed face's temperature is taken as ambient temperature for the entire heating period. The temperature at the exposed face rises from ambient temperature to the reference temperature in 3600 seconds such that the complete degradation starts at the exposed face at the reference heating time t_{ref} and moves inwards. Same as the panels discussed in the previous section, the single skin panel is made of E-glass/vinylester composite; the sandwich panel is made of E-glass/vinylester composite skin and *airlite* foam core. Thermal properties are taken to be temperature independent in this example. For the composites, the thermal conductivity is taken as $K = 0.25$ watt/(m °C); specific heat $C_p = 1500$ J/(kg °C); mass density $\rho = 1600$ kg/m³. For the *airlite* foam, the thermal conductivity is taken as $K_c = 0.16$ watt/(m °C); specific heat $C_{pc} = 1046$ J/(kg °C); mass density $\rho_c = 500$ kg/m³. These thermal properties may be found in Reference [10]. Mechanical properties are the same as those given in the previous section with Poisson's ratio of the core $\nu_{1c} = 0.33$ in the wrinkling load calculation. The dimensions of the panels are the same as those given in the previous section, except the width of panel b which is taken to be a unit value here. Both ends are considered to be roller-supported.

Fig. 12 shows buckling load versus heating time for the single skin panel. As expected, the buckling load decreases as the heating time increases. The buckling load decreases more rapidly after the exposed face reaches the reference temperature at 3600 seconds of the heating time. This descending behavior divides the curve into two portions. At 3600 seconds of the heating time, the panel loses 22% of the buckling load from its original load-bearing capability at the heating time equal to zero, whereas at 6000 seconds the loss is dramatically enlarged to 82%. This shows that the buckling load-bearing capability is strongly influenced by whether the panel reaches the reference temperature. This also tells that the mechanical performance is directly influenced by the thermal performance in the combined thermal–mechanical process. This observation makes the point on the design diagram denoted by (t_{ref}, P_{ref}) , where the heating time corresponds to the reference temperature at the exposed face, to be an important point.

Given the allowable mechanical load P_M from mechanical requirement in a design, one finds the fire protection time t_M in Fig. 12. Furthermore, from the fire protection time t_M , one finds the permitted temperature at the exposed side T_M in Fig. 11. On the other hand, given the allowable temperature at the exposed side T_T from thermal requirement in a design, one finds the fire protection time t_T in Fig. 11 and then the permitted mechanical load P_T in Fig. 12. The design procedure to locate the permitted temperature and mechanical load as well as fire protection time is done automatically by the computer program when the allowable values for a design are inputted.

We use the above result for single skin panel in Fig. 12 to illustrate the design procedure. If the design of buckling load without fire is based on a safety factor 1.5, the allowable compressive load for

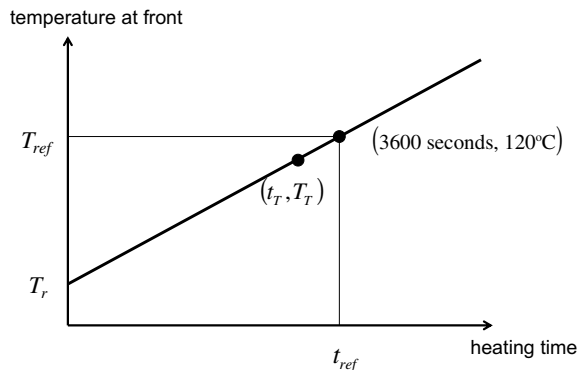


Fig. 11. A thermal boundary condition at the exposed face, temperature versus heating time. The time at which the temperature reaches the reference temperature T_{ref} is t_{ref} .

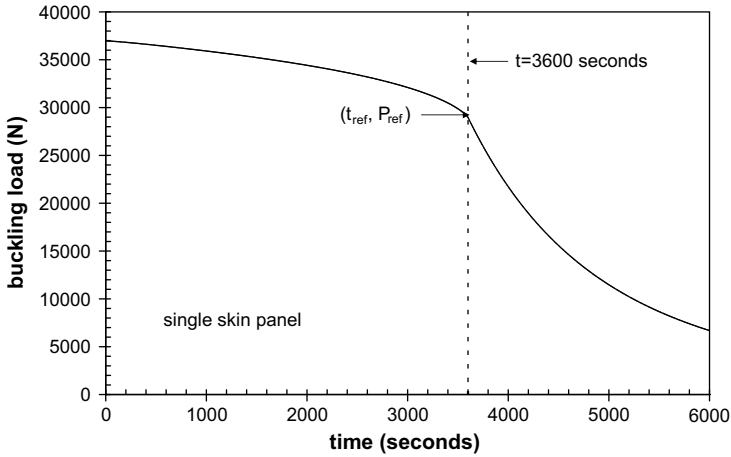


Fig. 12. Buckling load versus heating time for a single skin panel. After the exposed face reaches the reference temperature at $t = 3600$ seconds, the buckling load is reduced significantly.

the panel is the buckling load at heating time $t = 0$ divided by 1.5, i.e. $P_M = 24,651$ N. From the curve in Fig. 12 we find that this corresponds to the heating time $t_M = 3824$ seconds. This is to say that this mechanical load design gives 3824 seconds of fire protection time for the panel. From Fig. 11, we find the temperature allowed at the exposed face is $T_M = 126$ °C. On the other hand, the thermal consideration of a design may require the exposed face’s temperature to be less than an allowable value, say $T_T = 103$ °C, as shown in Fig. 11. Using T_T , the fire protection time $t_T = 3000$ seconds is located in Fig. 11. Then, one obtains the allowable compressive load $P_T = 32,104$ N in Fig. 12. From the above analysis, there are two ways to use the design diagram. One is to determine fire protection time from allowable mechanical load, and another is to determine allowable mechanical load from fire protection time. If a design is to place both mechanical load and temperature at the exposed face under allowable values, the actual fire protection time is

$$t = \min(t_M, t_T); \tag{31}$$

the actual allowable temperature at the exposed face is

$$T = \min(T_M, T_T); \tag{32}$$

the actual allowable mechanical load is

$$P = \min(P_M, P_T). \tag{33}$$

In this case, the actual allowable mechanical load is $P = 24,651$ N; the actual fire protection time is $t = 3000$ seconds, and the actual allowable temperature at the exposed face is $T = 103$ °C.

Fig. 13 shows buckling load versus heating time for the sandwich panel. Since the wrinkling load obtained is larger than the buckling load shown in the figure for the heating time period up to 4230 seconds, the sandwich panel’s failure is controlled by the buckling mechanism in this time period. After 4230 seconds, both the buckling load and the wrinkling load become very small. This is due to that the exposed skin is completely degraded to lose load-bearing capacity beyond that heating time. This suggested that, if the load-bearing capacity is the concern, this panel may not sustain external compression after 4230 seconds. The buckling load in Fig. 13 decreases more rapidly after the exposed face reaches the reference temperature at 3600 seconds of the heating time. This descending behavior divides the curve into two portions. At 3600 seconds of the heating time, the panel loses 26% of the buckling load from its original buckling load-bearing capability at heating time equal to zero, whereas at 4230 seconds the loss is dramatically enlarged to 99%. These qualitative and quantitative behaviors are similar to the single skin panel shown Fig. 12. Same as the single skin panel, we discuss a specified

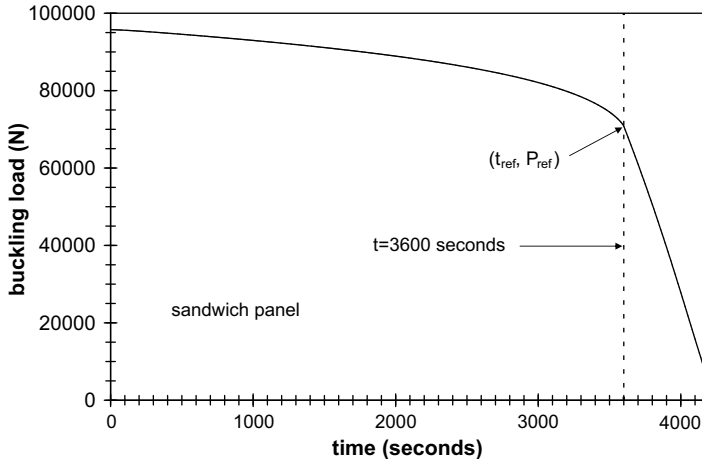


Fig. 13. Buckling load versus heating time for a sandwich panel. After the exposed face reaches the reference temperature at $t = 3600$ seconds, the critical load is reduced significantly.

design requirement. If the allowable mechanical load is specified as $P_M = 10,000$ N, the fire protection time given by the program is $t_M = 4149$ seconds and the permitted temperature at the exposed face is $T_M = 135$ °C. If the design specifies the allowable temperature at the exposed face is $T_T = 100$ °C, the fire protection is $t_T = 2880$ seconds and the permitted mechanical load is $P_T = 83,212$ N. If both above thermal and mechanical requirements are required to be satisfied, we have from Equations (31)–(33) that, the actual allowable temperature at the exposed face is $T = 100$ °C; the actual fire protection time is $t = 2880$ seconds; the actual allowable mechanical load is $P = 10,000$ N.

8. Discussions

In this paper, we discussed the stability issues of polymer matrix composite panels, single skin and sandwich panels, in fire. Temperature-dependent material behaviors of polymer matrix composites were modeled. The panels were subjected to the thermal–mechanical condition, i.e. in-plane compressive loads and transverse thermal gradients. Analytical solutions of buckling and skin wrinkling were discussed in detail for the purpose of exploring failure mechanisms and design considerations. The buckling solutions were discussed in the light of the thermal–mechanical tests performed for both single skin and sandwich panels. The comparison showed that the analytical solutions were in agreement with available data measured in tests.

The coupled, or combined, thermal–mechanical events were simulated by the chained thermal–mechanical numerical process. That is, at each time step, the transverse thermal field was obtained from the heat conduction equation using the thermal boundary conditions at the exposed face and unexposed face. Then, the obtained temperature field was substituted into the analytical solutions of buckling and wrinkling to determine the critical load. We made a computer program for the combined thermal–mechanical simulations, which produced design diagrams to locate allowable loads for given thermal and mechanical requirements. A procedure was illustrated to design the panel's mechanical load carrying capacity for given thermal requirement, and on the opposite, to design the panel's fire protection time for given allowable mechanical load. Using the design diagrams, one can find allowable mechanical load, allowable temperature at the boundaries and fire protection time, given the mechanical and thermal requirements.

Our focus here is the initial response of mechanical performance to fire in the temperature range, say < 120 °C, where the mechanical behavior of the polymer matrix composites is significant. The residual performance of the polymer matrix composites is not considered in this study. With the phase transition to the charred materials at higher temperature range in fire, the thermal conductivity of the

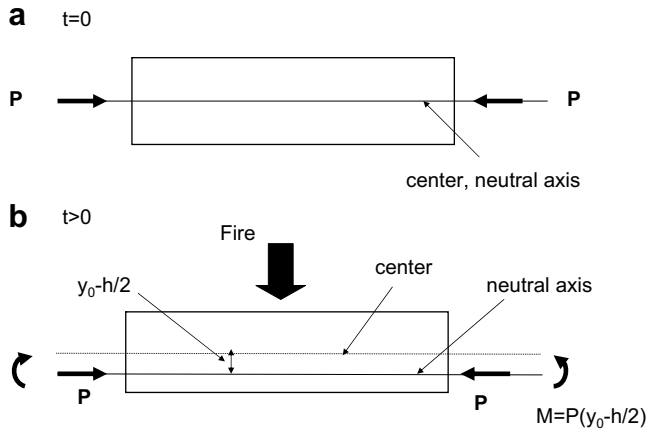


Fig. 14. The relocation of the neutral axis during fire. (a) At $t = 0$, the neutral axis is located at the center of the cross-section; (b) at $t > 0$, the shift of the neutral axis induces bending moment which causes bending deformation.

charred portion of composites is reduced significantly [22]. The goal is to develop a methodology for assessing the fire damage to the mechanical load-bearing capacity of the panels and thus designing the panel's structural integrity in fire.

In addition to the discussed buckling and skin wrinkling, other failure mechanisms exist. For such low thermal conductivity materials in the case without external mechanical loads, the transverse thermal gradient induces non-uniform thermal expansion along the thickness that results in transverse deformation field, referred as thermal distortion or warping. The deflection in the thermal distortion may exceed the design limit to fail structures. It was shown in Reference [12] that the thermal distortion is dependent of the material gradient induced by the thermal gradient along the thickness and the coefficient of thermal expansion. For linear temperature profile (two-parameter thermal model [9,10]), the thermal distortion was shown to be independent of the material variation along the thickness and the curvature of the deformed panel is given by the expression,

$$\kappa = -\frac{\alpha \Delta T}{h}. \tag{34}$$

Here, α is the coefficient of thermal expansion and ΔT is the temperature difference between the exposed face and the unexposed face. The influence of geometrical nonlinearity and material nonlinearity to the thermal distortion was investigated in References [23,24] using both analytical and numerical models.

The other issue is due to the change of the loading status at the two ends induced by the shift of the neutral axis in fire. The material gradient along the thickness induced by temperature gradient causes the neutral axis to move from the center of the cross-section according to the expression (5). At the beginning of the fire, the total force acting on the neutral axis at the two ends is the compressive force P . During fire, the total force acting on the relocated neutral axis at the two ends is the compressive force P plus a bending moment $M = P(y_0 - h/2)$, see Fig. 14. The bending moment M gives rise to additional deflection and internal stresses in the panels [17,18]. It was shown in these two references that, at a relatively long heating time, the critical load obtained from the failure criteria establishing from the bending deformation caused by the moment M can be lower than that from the buckling solution. This suggests that the actual allowable load at a longer heating time can be determined by the deformation mechanism of shifting neutral axis.

References

- [1] Couchman L, Mouritz AP, editors. Modeling of naval composite structures in fire. Templestowe, Victoria, Australia: Acclaim Printing; 2006.

- [2] Henderson JB, Wiebelt JA, Tant MR. A model for the thermal response of polymer composite materials with experimental verification. *Journal of Composite Materials* 1985;19:579–95.
- [3] Gibson AG, Wu Y-S, Chandler HW, Wilcox JAD, Bettess P. A model for the thermal performance of thick composite laminates in hydrocarbon fires. *Revue de L'Institut Francais du Petrole* 1995;50:69–74.
- [4] Mouritz AP, Mathys Z. Mechanical properties of fire-damaged glass-reinforced phenolic composites. *Fire and Materials* 2000;34:67–75.
- [5] Gibson AG, Wright PNH, Wu Y-S, Mouritz AP, Mathys Z, Gardiner CP. The integrity of polymer composites during and after fire. *Journal Composite Materials* 2004;38:1283–307.
- [6] Feih S, Mathys Z, Gibson AG, Mouritz AP. Modelling the compression strength of polymer laminates in fire. *Composites Part A* 2007;38:2354–65.
- [7] Feih S, Mouritz AP, Mathys Z, Gibson AG. Tensile strength modeling of glass fiber polymer composites in fire. *Journal of Composite Materials* 2007;41:2387–410.
- [8] Asaro RJ, Dao M. Fire degradation of fiber composites. *Marine Technology* 1997;34(3):197–210.
- [9] Dao M, Asaro RJ. A study on failure prediction and design criteria for fiber composites under fire degradation. *Composites Part A* 1999;30:123–31.
- [10] Asaro RJ, Dao M, Myskowski C. Structural fire safety of composite materials used on high speed craft as regulated by the IMO high speed craft code. Technical Report of Department of Structural Engineering, The University of California at San Diego; 1999.
- [11] Gu P, Asaro RJ. Structural buckling of polymer matrix composites due to reduced stiffness from fire damage. *Composite Structures* 2005;69:65–75.
- [12] Gu P, Asaro RJ. Distortion of polymer matrix composite panels under transverse thermal gradients. *Composite Structures* 2008;82:413–21.
- [13] Gu P, Asaro RJ. Wrinkling of sandwich polymer matrix composite panels under transverse thermal gradients. *Fire Safety Journal* 2008;43:151–60.
- [14] Asaro RJ, Krysl P, Ramroth WT. Structural fire integrity of FRP composites: analysis and design. In: Couchman L, Mouritz AP, editors. *Modeling of naval composite structures in fire*. Templestowe, Victoria, Australia: Acclaim Printing; 2006.
- [15] Asaro RJ, Krysl P, Zhu B, Ramroth WT. Rate dependent constitutive modeling of laminated FRP composites degraded by fire. *Composite Structures* 2005;68:399–408.
- [16] Krysl P, Ramroth WT, Stewart LK, Asaro RJ. Finite element modeling of fiber reinforced polymer sandwich panels exposed to heat. *International Journal for Numerical Methods in Engineering* 2004;61:49–68.
- [17] Gu P, Asaro RJ. Designing polymer matrix composite panels for structural integrity in fire. *Composite Structures* 2008;84:300–9.
- [18] Gu P, Asaro RJ. Designing sandwich polymer matrix composite panels for structural integrity in fire. *Composite Structures* 2009;88:461–7.
- [19] Bausano JV, Lesko JJ, Case SW. Composite life under sustained compression and one sided simulated fire exposure: characterization and prediction. *Composites Part A* 2006;37:1092–100.
- [20] Allen HG. Analysis and design of structural sandwich panels. New York, NY: Pergamon Press; 1969.
- [21] Hollaway LC, Head PR. *Advanced polymer composites and polymers in the civil infrastructure*. Amsterdam, Netherlands: Elsevier; 2001.
- [22] Asaro RJ, Lattimer B, Mealy C, Steele G. Thermo-physical performance of a fire protective coating for naval ship structures. *Composites Part A*, 2009;40:11–8.
- [23] Birman V, Kardomateas GA, Simites GJ, Li R. Response of a sandwich panel subject to fire or elevated temperature on one of the surfaces. *Composites Part A* 2006;37:981–8.
- [24] Gu P, Asaro RJ. Influence of material nonlinearity on thermal distortion of polymer matrix composite panels, in preparation.